ARTICLE Communicated by Carl van Vreeswijk

Synchronization of the Neural Response to Noisy Periodic Synaptic Input

A. N. Burkitt
a.burkitt@medoto.unimelb.edu.au
Bionic Ear Institute, East Melbourne, Victoria 3002, Australia

G. M. Clark
g.clark@medoto.unimelb.edu.au
Department of Otolaryngology, Bionic Ear Institute and University of Melbourne, Royal Victorian Eye and Ear Hospital, East Melbourne, Victoria 3002, Australia

The timing information contained in the response of a neuron to noisy periodic synaptic input is analyzed for the leaky integrate-and-fire neural model. We address the question of the relationship between the timing of the synaptic inputs and the output spikes. This requires an analysis of the interspike interval distribution of the output spikes, which is obtained in the gaussian approximation. The conditional output spike density in response to noisy periodic input is evaluated as a function of the initial phase of the inputs. This enables the phase transition matrix to be calculated, which relates the phase at which the output spike is generated to the initial phase of the inputs. The interspike interval histogram and the period histogram for the neural response to ongoing periodic input are then evaluated by using the leading eigenvector of this phase transition matrix. The synchronization index of the output spikes is found to increase sharply as the inputs become synchronized. This enhancement of synchronization is most pronounced for large numbers of inputs and lower frequencies of modulation and also for rates of input near the critical input rate. However, the mutual information between the input phase of the stimulus and the timing of output spikes is found to decrease at low input rates as the number of inputs increases. The results show close agreement with those obtained from numerical simulations for large numbers of inputs.

1 Introduction

The degree of phase locking in the response of neurons to noisy periodic synaptic input plays an important role in auditory processing and has been studied for a considerable time (Gerstein & Kiang, 1960; Rose, Brugge, Anderson, & Hind, 1967). Gerstein and Kiang presented an auditory stimulus to anesthetized cats and observed a multimodal interspike interval

histogram (ISIH), resulting from spikes that tend to fire near the peak of the stimulus and hence cluster around integer multiples of the stimulus period. Rose and colleagues analyzed the phase-locked responses in terms of the phase histogram, in which the responses are plotted in terms of their relation to the phase of the stimulus. Subsequent authors extended this work to examine the relationship between the spike rate and synchrony of the response of auditory neurons to low- and midfrequency single tones (Anderson, 1973; Johnson, 1980). The neural responses to acoustical stimuli in cats indicated that spikes are phase locked up to around 3–5 kHz in mammals (Rose et al., 1967; Johnson, 1980) and up to frequencies of 8 kHz in the barn owl (Köppl, 1997). This behavior was simulated using a Monte Carlo simulation of the diffusion equation with a periodically varying drift parameter (Gerstein & Mandelbrot, 1964), and ISIHs were obtained that resembled the experimental results. In this same article, Gerstein and Mandelbrot gave an analytical solution to the integrate-and-fire neural model in which the decay of the potential across the cell membrane is ignored; this is called the perfect integrator neural model. Although this is clearly an unphysiological approximation, it nevertheless provides a description that captures some of the characteristics of the spontaneous activity in auditory nerve fibers (Gerstein & Mandelbrot, 1964; Iyengar & Liao, 1997). However, Monte Carlo simulations were required to compare the theory with experiment when acoustic stimuli were presented. The results of the simulations showed many of the same features as the experimental data, including the multimodal peaks of the ISIHs (Gerstein & Mandelbrot, 1964).

One of the simplest and most widely used class of neural models capable of capturing this behavior is the integrate-and-fire model, first introduced by Lapicque (1907). In this class of models, the synaptic inputs produce a postsynaptic response of the membrane potential, which passively propagates to the soma, where a spike is generated when the summed contributions exceed a voltage threshold. The models typically lack any of the specific currents that underlie spiking, and thus the complex mechanisms by which the sodium and potassium conductances cause action potentials to be generated are not part of the model. Pulse-based models have, however, been developed in which the time courses of the rate constants are approximated by a pulse, and such models bridge the divide between the classical integrate-and-fire models and the Hodgkin-Huxley models (Destexhe, 1997). An important assumption is also that the synaptic inputs interact only in a linear manner, so that phenomena involving nonlinear interaction of synaptic inputs, such as pulse-paired facilitation-depression and synaptic inputs that depend on postsynaptic currents, are neglected. Nevertheless, a comparison of the integrate-and-fire model with the Hodgkin-Huxley model when both receive a stochastic input current found that the threshold model provides a good approximation (Kistler, Gerstner, & van Hemmen, 1997). A recent review of the integrate-and-fire neural model that provides details of the

variations of the model and comparisons with both experimental data and other models is given in Koch (1999).

An analysis of the integrate-and-fire model with periodic input, using a deterministic differential equation without any noise, found three regions in parameter space (the space defined by the frequency of synaptic inputs, average rate of inputs, synchronization of inputs, and the time constant of the membrane potential decay) with distinctly different behaviors (Keener, Hoppensteadt, & Rinzel, 1981): a phase-locking region, a region with apparently nonperiodic behavior, and a region where the firing eventually dies out. This extended earlier studies on systems with a deterministic response to sinusoidal stimuli (Rescigno, Stein, Purple, & Poppele, 1970; Stein, French, & Holden, 1972), and a study of phase locking in which the threshold was sinusoidally modulated (Glass & Mackey, 1979). Subsequent work on the effect of a periodically varying rate of input to noisy integrate-and-fire neurons has focused largely on stochastic counterparts to this approach, using either numerical simulations, such as in the study of the temporal acuity and localization in the barn owl auditory system (Gerstner, Kempter, van Hemmen, & Wagner, 1996), or stochastic differential equations (Bulsara, Elston, Doering, Lowen, & Lindenberg, 1996; Lánský, 1997).

Much of the recent work on the response of neural systems to noisy periodic synaptic input has been motivated by an interest in the applicability of stochastic resonance to these systems, in which the detection of a subthreshold periodic stimulus is enhanced by the presence of noise (Fauve & Heslot, 1983). Stochastic resonance has been extensively studied by analyzing the effect of a noisy weak periodic stimulus on a system in a double-well potential, a review of which is given in Gammaitoni, Hänggi, Jung, & Marchesoni (1998). The phenomenon of stochastic resonance was demonstrated in neural systems by using external noise applied to crayfish mechanoreceptor cells (Douglas, Wilkens, Pantozelou, & Moss, 1993), and this generated considerable interest in the analysis of stochastic resonance in neural models (Longtin, 1993; Stemmler, 1996; Chialvo, Longtin, & Müller-Gerking, 1997). However, much of this work involved the analysis of the more mathematically tractable situation in which the phase of the input stimulus is reset after each output spike is generated (Plesser & Tanaka, 1997), a situation that is implausible in the neurophysiological context. A method for solving this shortcoming has recently been proposed (Plesser & Geisel, 1999a, 1999b; Shimokawa, Pakdaman, & Sato, 1999) in which the spike output distribution is considered a function of the phase of the stimulus at which both the summation is initiated and the output spike is generated. Consequently, it is possible to find the stationary spike phase distribution—the average phase distribution—that results over the whole time course of the periodic stimulus (Hohn & Burkitt, 2001).

A further impetus to the study of periodic synaptic inputs has been the observation of synchronized periodical activity of neurons in various brain areas, such as the oscillations observed in the visual cortex (Eckhorn et al.,

1988; Gray, König, Engel, & Singer, 1989). This has led to the hypothesis that synchronized activity of neurons may play a role in brain functioning, such as pattern segmentation and feature binding (von der Malsburg & Schneider, 1986; Eckhorn et al., 1988; Gray & Singer, 1989; Singer, 1993; Usher, Schuster, & Niebur, 1993). It has also been proposed that the information contained in a spike sequence could be coded using the relationship between the spike times and the oscillation of the periodic background signal (Hopfield, 1995; Jensen & Lisman, 1996; Tsodyks, Skaggs, Sejnowski, & McNaughton, 1996).

In a recent article (Kempter, Gerstner, van Hemmen, & Wagner, 1998), the response of an integrate-and-fire neuron to noisy periodic spike input is studied, and a thorough analysis of the relationship between the input and output rates over the range of input vector strengths (also called the synchronization index) is carried out. Their results show how the output rate increases with both the input rate and synchrony and how it depends on the neural parameters, such as the threshold, the number of synapses, and the time course of the postsynaptic response to the inputs. They are also able to identify the conditions under which a neuron can act as a coincidence detector and thus convert a temporal code into a rate code. They identify two parameters—the coherence gain (which provides a measure of the mean output firing rate for synchronized versus random input) and the quality factor for coincidence detection (which provides a measure of the difference in the neural response to random and synchronized inputs)—which largely characterize the performance of a coincidence detector, and they plot these quantities for representative values of the neural parameters over the range of input vector strengths. However, since their analysis concerns only the output rate, they are not able to predict quantities that depend on the details of the timing of individual output spikes.

In this article, we provide an important extension of these results by analyzing the time distribution of output spikes in response to noisy periodic synaptic input, that is, the probability of an output spike's being produced at a particular phase of the periodic input. Our analysis enables us to find the interspike interval distribution of the output spikes, the synchronization index of the outputs, and the phase distribution of the outputs. In order to examine the amount of information that the output spikes carry about the stimulus, the mutual information between the input phase of the stimulus and the timing of output spikes is calculated. The analysis is carried out in the gaussian approximation, in which the amplitude of the postsynaptic response to an individual input spike is small, similar to the diffusion approximation (Tuckwell, 1988a). For neurons with large numbers of small-amplitude inputs, this approximation proves to be very accurate, as will be discussed in section 3.2, where the results are compared with numerical simulations.

In the following section, we give an outline of the model, including the neural model (in section 2.1) and the synaptic input (in section 2.2). In order

to calculate the interspike interval (ISI) distribution, it is first necessary to calculate the probability density of the membrane potential, which is done in section 2.3. The ISI distribution is then calculated in two steps: first by calculating the conditional ISI distribution (i.e., conditional on the initial phase of the inputs) in section 2.4 and then by forming the appropriate average over the initial phases in section 2.5. The calculation of the mutual information between the input phase and the timing of output spikes is outlined in section 2.6. The typical ISI distributions obtained are illustrated in section 3.1. The synchronization index is analyzed in section 3.2, and the results of the calculation of the mutual information are presented in section 3.3. The results are discussed in section 4. The appendixes contain an exact analysis of the ISI distribution for the perfect integrator model with noisy periodic synaptic input.

2 Methods

In this section, we calculate the ISI distribution and the phase distribution for the leaky integrate-and-fire neural model. The notation follows that in Burkitt and Clark (1999, 2000), with the straightforward generalization to include the frequency and phase of the periodic synaptic input, as described below.

2.1 Neural Model. In the analysis presented here, we consider a single neuron with N independent inputs (afferent fibers), labeled with index k. The membrane potential is assumed to be reset to its initial value at time $t = 0$, $V(0) = v_0$ after an action potential (AP) has been generated. An AP (spike) is produced only when the membrane voltage exceeds the threshold, $V_{\rm th}$, which has a potential difference with the reset potential of $\theta = V_{\rm th} - v_0$. The potential is the sum of the excitatory and inhibitory postsynaptic potentials (EPSPs and IPSPs, respectively),

$$V(t) = v_0 + \sum_{k=1}^{N} a_k s_k(t), \qquad s_k(t) = \sum_{m=1}^{\infty} u_k(t - t_{k_m}), \tag{2.1}$$

where the index $k = 1, \ldots, N$ denotes the afferent fiber and the index m denotes the mth input from the particular fiber, whose time of arrival is t_{k_m} ($0 < t_{k_1} < t_{k_2} < \cdots < t_{k_m} < \cdots$). The amplitude of the inputs from fiber k is a_k, which is positive for EPSPs and negative for IPSPs, and the time course of an input at the site of spike generation is described by the synaptic response function $u_k(t)$ for the leaky integrate-and-fire model. The results we present here are for the shot-noise model, where the synaptic response function is

$$u_k(t) = \begin{cases} e^{-t/\tau} & \text{for } t \geq 0 \\ 0 & \text{for } t < 0, \end{cases} \tag{2.2}$$

where τ is the time constant of the membrane potential. Consequently, the membrane potential has a discontinuous jump of amplitude a_k upon the arrival of an EPSP and then decays exponentially between inputs. The decay of the EPSP across the membrane means that the contribution from EPSPs that arrive earlier has partially decayed by the time that later EPSPs arrive. The natural unit of time is the membrane time constant, τ, and other units of time such as the period of the inputs, $T = 2\pi/\omega$, are given here in units of τ. Synaptic response functions with an arbitrary time course may also be analyzed, which may allow a more accurate model of the time course of the incoming EPSP. The above synaptic response function, equation 2.2, is identical for all inputs, but the analysis also allows response functions with different time courses for different input fibers. This enables, for example, the effect of propagation of the PSPs along the dendritic tree to be modeled for inputs with synapses at different distances from the site at which the neuron generates an action potential (typically the axon hillock).

2.2 Synaptic Input. The degree of phase locking (or synchronization) is measured by the vector strength r (Goldberg & Brown, 1969), also known as the synchronization index (Anderson, 1973; Johnson, 1980),

$$\begin{aligned} r &= \left(r_S^2 + r_C^2\right)^{1/2} \\ r_S &= \frac{1}{N}\sum_{m=0}^{M-1} h_m \sin\left(\frac{2\pi m}{M}\right) \\ r_C &= \frac{1}{N}\sum_{m=0}^{M-1} h_m \cos\left(\frac{2\pi m}{M}\right), \end{aligned} \tag{2.3}$$

where here h_m denotes the number of spikes in the mth bin of a period histogram with M bins and N denotes the total number of spikes ($N = \sum h_m$). The vector strength takes values between zero (a flat period histogram) and one (all spikes in one bin of the period histogram). We assume that the input rate on each of the input fibers is identical. The time-dependent rate of arrival of input spikes at a synapse is periodic with frequency ω and initial phase ϕ_{in}, that is, the phase of the input at the time when the summation commences,

$$\lambda(t) = \bar{\lambda}_{\text{in}}\left(1 + 2r_{\text{in}}\cos(\omega t + \phi_{\text{in}})\right), \qquad 0 \le r_{\text{in}} \le 0.5, \tag{2.4}$$

where $\bar{\lambda}_{\text{in}}$ is the time-averaged input rate on a single fiber and r_{in} is the synchronization index of the input spikes. With this parameterization of the input rate, the value $r_{\text{in}} = 0.5$ represents a highly modulated input, and values of r_{in} closer to zero represent inputs that contain less of the frequency-dependent component (the requirement that the rate be nonneg-

ative restricts r_{in} to the interval [0, 0.5] with this parameterization). Frequency and rate are given in units of the membrane time constant (as cycles or spikes per unit of the membrane time constant τ), and the frequency and average rate of the inputs can be varied independently. The use of the term *frequency* here and throughout the rest of the analysis refers to this periodic modulation of the rate of inputs (it is not synonymous with the average rate of inputs). This input rate function represents an inhomogeneous (i.e., nonstationary) Poisson process (Papoulis, 1991). Other inhomogeneous Poisson rate models of periodic synaptic input have also been examined in the literature, such as modeling the rate with a sum of gaussian distributions with centers separated by the mean period and the width chosen to give the required synchronization index (Kempter et al., 1998; appendix A of their article summarizes the properties of the inhomogeneous Poisson process).

2.3 The Probability Density of the Potential. The probability density of the potential $V(t)$ is denoted by $p(v, t \mid v_0; \omega, \phi)$, which is the probability that the potential has the value v at time t, given the initial condition is $V(0) = v_0$, the frequency of the input is ω, and the initial phase is ϕ. This initial condition corresponds to the reset of the membrane potential to v_0 immediately after the previous spike, which is assumed to occur at time $t = 0$. The probability density is given by the following normalized expectation value, which is the integrated average over the time distribution of synaptic inputs (Burkitt & Clark, 1999, 2000),

$$p(v, t \mid v_0; \omega, \phi) = \mathrm{E}\{\delta(V(t) - v)\}, \tag{2.5}$$

where $\delta(x)$ is the Dirac delta function and the expectation value is over the (random) time of arrival of the synaptic inputs. The frequency and phase dependence of the probability density arise through this averaging over the arrival times of the synaptic input, which is described here explicitly by $\lambda(t)$, equation 2.4. Using the Fourier integral representation of the Dirac delta function, the probability density may be written as

$$\begin{aligned} & p(v, t \mid v_0; \omega, \phi) \\ &= \int_{-\infty}^{\infty} \frac{dx}{2\pi} \exp\{ix(v - v_0)\} \mathrm{E}\left\{\exp\left(-ix \sum_{k=1}^{N} a_k s_k(t)\right)\right\} \\ &= \int_{-\infty}^{\infty} \frac{dx}{2\pi} \exp\{ix(v - v_0)\} \prod_{k=1}^{N} F_k(x, t; \omega, \phi) \\ &= \int_{-\infty}^{\infty} \frac{dx}{2\pi} \exp\left\{ix(v - v_0) + \sum_{k=1}^{N} \ln F_k(x, t; \omega, \phi)\right\}, \end{aligned} \tag{2.6}$$

where the function $F_k(x, t; \omega, \phi)$ is given by

$$F_k(x, t; \omega, \phi) = \mathrm{E}\left\{\exp\left(-ixa_k s_k(t)\right)\right\}, \tag{2.7}$$

and we have used the independence of the contributions from each afferent fiber to obtain the product of F_k's in equation 2.6. Expanding the exponential in powers of a_k, we obtain

$$\begin{aligned}
&\ln F_k(x, t; \omega, \phi) \\
&\quad = \ln \mathrm{E}\left\{1 - ixa_k s_k(t) - \frac{x^2 a_k^2}{2} s_k^2(t) + O(a_k^3)\right\} \\
&\quad = \ln\left[1 - ixa_k \mathrm{E}\{s_k(t)\} - \frac{x^2 a_k^2}{2}\mathrm{E}\left\{s_k^2(t)\right\} + O(a_k^3)\right] \\
&\quad = -ixa_k \mathrm{E}\{s_k(t)\} - \frac{x^2 a_k^2}{2}\left[\mathrm{E}\left\{s_k^2(t)\right\} - (\mathrm{E}\{s_k(t)\})^2\right] + O(a_k^3),
\end{aligned} \tag{2.8}$$

where $O(y)$ denotes a remainder term that is smaller than $C \times |y^3|$ when y lies in a neighborhood of 0 for some positive constant C. We carry out the analysis in the gaussian approximation and henceforth neglect the $O(a_k^3)$ terms. This expansion to second order in powers of a_k is an approximation, which allows the resulting equations to be solved formally, and we do not address questions such as the convergence of the expansion. The accuracy of the results obtained will be compared in section 3.2 with those obtained using numerical simulation in order to gain confidence in our method and results. We expect the approximation to work best for large values of N and values of the amplitudes of the postsynaptic potential (PSP) that are small (voltage is measured in units of the difference θ between the threshold, V_{th}, and reset, v_0, potentials). In many neurons, this approximation provides an accurate description (Abeles, 1991; Douglas & Martin, 1991).

The probability density function is evaluated as

$$\begin{aligned}
&p(v, t \mid v_0; \omega, \phi) \\
&\quad = \int_{-\infty}^{\infty} \frac{dx}{2\pi} \exp\left\{ix\left(v - v_0 - \Upsilon(t; \omega, \phi)\right) - \frac{x^2}{2}\Gamma(t; \omega, \phi)\right\} \\
&\quad = \frac{1}{\sqrt{2\pi\Gamma(t; \omega, \phi)}} \exp\left\{-\frac{(v - v_0 - \Upsilon(t; \omega, \phi))^2}{2\Gamma(t; \omega, \phi)}\right\},
\end{aligned} \tag{2.9}$$

with

$$\Upsilon(t; \omega, \phi) = \sum_{k=1}^{N} a_k \mathrm{E}\{s_k(t)\},$$

$$\Gamma(t;\omega,\phi) = \sum_{k=1}^{N} a_k^2 \left(\mathrm{E}\left\{ s_k^2(t) \right\} - (\mathrm{E}\{s_k(t)\})^2 \right). \tag{2.10}$$

This expression ensures that $\Gamma(t;\omega,\phi) > 0$ for cases of interest. These expressions allow inputs with arbitrary amplitude distributions, including inhibitory inputs, to be considered. However, for simplicity, we consider here the situation where the postsynaptic potentials from the inputs are all excitatory and equal in both amplitude, $a_k = a > 0$, and time course, $u_k(t) = u(t)$, and where the rates on each of the N afferent fibers are identical, $\lambda_k(t) = \lambda(t)$. Consequently, we drop the index k in the following section, since all input fiber characteristics are identical. In the case of an inhomogeneous Poisson process with rate $\lambda(t)$ on each fiber, the expressions for $\Upsilon(t;\omega,\phi)$ and $\Gamma(t;\omega,\phi)$ take the forms (Papoulis, 1991)

$$\begin{aligned}
\Upsilon(t;\omega,\phi) &= Na\mathrm{E}\{s(t)\} = Na\int_0^t \lambda(t')u(t-t')dt', \\
\Gamma(t;\omega,\phi) &= Na^2\left(\mathrm{E}\left\{ s^2(t) \right\} - (\mathrm{E}\{s(t)\})^2 \right) \\
&= Na^2 \int_0^t \lambda(t')u^2(t-t')dt'.
\end{aligned} \tag{2.11}$$

The dependence of the expressions for $\Upsilon(t;\omega,\phi)$ and $\Gamma(t;\omega,\phi)$ above on frequency and initial phase is therefore given explicitly through the dependence on $\lambda(t)$ (refractory effects are ignored here, but a method for incorporating them is given in section 4).

2.4 First-Passage Time to Threshold. In order to calculate the probability density of output spikes, it is necessary to find the time at which a spike is generated—the time at which the summed membrane potential crosses the threshold, $V_{\mathrm{th}} = v_0 + \theta$, for the first time (called the *first-passage time*). The conditional first-passage time to threshold density, $f_\theta(t;\omega,\phi)$, which depends on the frequency, ω, and phase, ϕ, of the synaptic input, is obtained from the integral equation (Plesser & Tanaka, 1997; Burkitt & Clark, 1999) (for $v \geq V_{\mathrm{th}}$)

$$p(v,t|v_0;\omega,\phi) = \int_0^t dt' f_\theta(t';\omega,\phi)\hat{p}(v,t \mid V_{\mathrm{th}},t',v_0) \tag{2.12}$$

where $\hat{p}(v_2,t_2 \mid v_1,t_1,v_0)$ is an approximation to the conditional probability density of the potential. The conditional probability density, $p(v_2,t_2 \mid v_1,t_1,v_0)$, is defined as the probability that the potential has the value v_2 at time t_2, given that $V(t_1) = v_1$ and the reset value of the potential after a spike is v_0. Our approximation to the conditional probability density, $\hat{p}(v_2,t_2 \mid v_1,t_1,v_0)$, has the same definition with the added restriction that

the potential is subthreshold in the time interval $0 \leq t < t_1$. If the fluctuations in the input currents are not temporally correlated, then the approximate expression is exact, as is the case for both the perfect integrator model and the shot-noise model (see equation 2.2). However, the two expressions will differ if there are temporal correlations, which occurs if the presynaptic spikes have correlations or the synaptic currents have a finite duration. This conditional probability density clearly depends on ω and ϕ, such that in every case, the phase ϕ' associated with a particular time t' is given by $\phi' = [\omega t' + \phi]_{\mathrm{mod} 2\pi}$, where ϕ is the initial phase (at time $t = 0$). This gives a direct and straightforward correspondence between times, t, and phases, ϕ, of the input. Therefore, for notational convenience, the dependence of every quantity on the frequency and phase will be left implicit in this section. Note that equation 2.12, makes no assumptions about the stationarity of the conditional probability density (it does not require time-translational invariance).

The conditional probability density is given by

$$p(v_2, t_2 \mid v_1, t_1, v_0) = \frac{p(v_2, t_2, v_1, t_1 \mid v_0)}{p(v_1, t_1 \mid v_0)}, \tag{2.13}$$

and the joint probability density $p(v_2, t_2, v_1, t_1 \mid v_0)$, which is the probability that $V(t)$ takes the value v_1 at time t_1 *and* takes the value v_2 at time t_2 (given that the reset value of the potential after a spike is generated is again at v_0), may be evaluated (Burkitt & Clark, 2000):

$$\begin{aligned} p(v_2, t_2, v_1, t_1 \mid v_0) &= \mathrm{E}\left\{\delta(V(t_1) - v_1)\delta(V(t_2) - v_2)\right\} \\ &= \int_{-\infty}^{\infty} \frac{dx_2}{2\pi} \int_{-\infty}^{\infty} \frac{dx_1}{2\pi} \exp\left\{ix_2(v_2 - v_0)\right. \\ &\quad \left. + ix_1(v_1 - v_0) + N \ln F(x_2, x_1, t_2, t_1)\right\}, \end{aligned} \tag{2.14}$$

where

$$F(x_2, x_1, t_2, t_1) = \mathrm{E}\left\{\exp\left(-ix_2 a s(t_2) - ix_1 a s(t_1)\right)\right\}. \tag{2.15}$$

The function $\ln F(x_2, x_1, t_2, t_1)$ is expanded in the amplitude a of the synaptic response function as before (see equation 2.8) and contains cross-terms in $x_2 x_1$:

$$\begin{aligned} &\ln F(x_2, x_1, t_2, t_1) \\ &\quad = \ln \mathrm{E}\left\{1 - iax_2 s(t_2) - iax_1 s(t_1) - \frac{x_2^2}{2} a^2 s^2(t_2) - \frac{x_1^2}{2} a^2 s^2(t_1)\right. \\ &\qquad \left. - x_2 x_1 a^2 s(t_2) s(t_1) + O(a^3)\right\} \end{aligned}$$

$$= -ix_2 a\mathrm{E}\{s(t_2)\} - ix_1 a\mathrm{E}\{s(t_1)\}$$
$$- \frac{x_2^2}{2}a^2\left(\mathrm{E}\{s^2(t_2)\} - (\mathrm{E}\{s(t_2)\})^2\right) - \frac{x_1^2}{2}a^2\left(\mathrm{E}\{s^2(t_1)\} - (\mathrm{E}\{s(t_1)\})^2\right)$$
$$- x_2x_1a^2\left(\mathrm{E}\{s(t_2)s(t_1)\} - \mathrm{E}\{s(t_2)\}\mathrm{E}\{s(t_1)\}\right) + O(a^3). \tag{2.16}$$

The integrals in equation 2.14 may be evaluated in the gaussian approximation (Burkitt & Clark, 2000) by making the change of variable $y_1 = x_1 + \kappa(t_2, t_1)x_2$ where $\kappa(t_2, t_1)$ is chosen in order to eliminate the cross-term x_2y_1,

$$\kappa(t_2, t_1) = \frac{\mathrm{E}\{s(t_2)s(t_1)\} - \mathrm{E}\{s(t_2)\}\mathrm{E}\{s(t_1)\}}{\mathrm{E}\{s^2(t_1)\} - (\mathrm{E}\{s(t_1)\})^2} = \frac{C(t_2, t_1)}{C(t_1, t_1)}, \tag{2.17}$$

where $C(t_2, t_1)$ is the autocovariance of $s(t)$. In the case of an inhomogeneous Poisson process with rate $\lambda(t)$ on each fiber, the autocovariance of $s(t)$ is (Papoulis, 1991)

$$C(t_2, t_1) = \int_0^{t_1} \mathrm{d}t'\lambda(t')u(t_1 - t')u(t_2 - t'), \qquad t_2 \geq t_1. \tag{2.18}$$

The y_1 and x_2 integrals are now independent gaussian integrals and may be evaluated. The y_1 integral yields exactly $p(v_1, t_1|v_0, \omega, \phi)$, and the x_2 integral gives the conditional probability density,

$$p(v_2, t_2 \mid v_1, t_1, v_0)$$
$$= \frac{1}{\sqrt{2\pi\gamma\,(t_2, t_1)}}$$
$$\times \exp\left\{-\frac{[(v_2 - v_0 - \Upsilon(t_2) - \kappa(t_2, t_1)(v_1 - v_0 - \Upsilon(t_1))]^2}{2\gamma\,(t_2, t_1)}\right\}, \tag{2.19}$$

where

$$\gamma\,(t_2, t_1) = \Gamma(t_2) - \kappa^2(t_2, t_1)\Gamma(t_1)$$
$$= Na^2\frac{C(t_2, t_2)C(t_1, t_1) - C^2(t_2, t_1)}{C(t_1, t_1)}, \tag{2.20}$$

which ensures that $\gamma\,(t_2, t_1)$ is positive definite.

Equation 2.12, which defines the conditional first passage-time density, is a Volterra integral equation, which may be numerically evaluated using standard methods (Press, Flannery, Teukolsky, & Vetterling, 1992; Plesser & Tanaka, 1997) or variations on standard methods (details of the actual method used here are found in appendix B).

The solution of the perfect integrator version of the integrate-and-fire model, in which the decay of the potential across the membrane is neglected (or equivalently the membrane time constant is effectively infinite in comparison to the other timescales of the problem), is given in appendix A.

2.5 The Spike Phase Distribution and Synchronization Index. In the case of homogeneous Poisson inputs, the first passage-time density is identical with the interspike interval density. However, in the case of inhomogeneous Poisson inputs, this is no longer the case, except in the (unbiological) situation in which the phase of the input resets after each output spike is generated. It is therefore necessary now to examine explicitly the dependence of the conditional first-passage time density (the ISI distribution) on the phase of the input. In order to find the interspike interval density $\rho(t; \omega)$ generated by inhomogeneous Poisson inputs with period ω, it is necessary to form the appropriate average over the initial phases ϕ of the conditional first passage-time densities (Plesser & Geisel, 1999a, 1999b),

$$\rho(t; \omega) = \int_0^{2\pi} d\phi f_\theta(t; \omega, \phi)\chi^{(s)}(\phi), \tag{2.21}$$

where $\chi^{(s)}(\phi)$ is the stationary distribution of phases, evaluated as follows (Plesser & Geisel, 1999a). A phase transition density may be defined by

$$g(\phi', \phi) = \int_0^{\infty} dt f_\theta(t; \omega, \phi)\delta([\omega t + \phi]_{\mathrm{mod}2\pi} - \phi'), \tag{2.22}$$

which gives the probability density for output spikes with phase ϕ' when the initial phase is ϕ. Therefore, defining $\chi^{(n)}(\phi)$ to be the output spike phase density for the nth spike,

$$\chi^{(n+1)}(\phi') = \int_0^{2\pi} d\phi g(\phi', \phi)\chi^{(n)}(\phi), \tag{2.23}$$

and the stationary spike phase density, $\chi^{(s)}(\phi)$, is given by the (nontrivial) solution of

$$\chi^{(s)}(\phi') = \int_0^{2\pi} d\phi g(\phi', \phi)\chi^{(s)}(\phi). \tag{2.24}$$

By discretizing the phase axis, the phase transition density, $g(\phi', \phi)$, becomes a transition matrix $g_{\phi',\phi}$ and the stationary spike phase distribution vector, $\chi^{(s)}_\phi$, is the eigenvector corresponding to the eigenvalue 1 (Plesser & Geisel, 1999a).

2.6 Mutual Information Calculation. In addition to the interspike interval distribution, we would like to know the amount of information that the neural response (i.e., the spike times) contains about the phase of the periodic stimulus. The distribution of the input phase, ϕ_{in}, can be assumed to be uniform between 0 and 2π. We wish to determine the amount of information gained about the input phase of the stimulus when the output is observed for one cycle, and we consider the situation in which the neuron fires at most 1 spike per cycle (in the regime in which we are interested, this will be the case, as will be discussed in section 3). Consequently, it is necessary to evaluate only the probability of firing no spike, p_0, or firing one spike, p_1. In the general case, in which the output rate of firing is described by $\lambda_{\text{out}}(t)$, the probability p_0 is given by (Papoulis, 1991)

$$p_0 = \exp\left[-\int_0^T \lambda_{\text{out}}(t)dt\right]. \tag{2.25}$$

For small values of the average output rate, $\overline{\lambda}_{\text{out}}$ (defined as the number of spikes per unit time averaged over one cycle), this gives the probability of firing a spike, p_1, of $\overline{\lambda}_{\text{out}}/\omega$. The probability of firing a spike at phase ϕ_{out}, given that the input has a phase ϕ_{in}, is given by

$$P(\phi_{\text{out}}|\phi_{\text{in}}) = \overline{\lambda}_{\text{out}}\chi^{(s)}(\phi_{\text{out}} - \phi_{\text{in}})/(2\pi\omega). \tag{2.26}$$

The mutual information I_M is given by (Cover & Thomas, 1991)

$$I_M = \int_0^{2\pi} d\phi_{\text{out}} \int_0^{2\pi} \frac{d\phi_{\text{in}}}{2\pi} P(\phi_{\text{out}}|\phi_{\text{in}}) \log_2(P(\phi_{\text{out}}|\phi_{\text{in}})) - \int_0^{2\pi} d\phi_{\text{out}} \overline{P}(\phi_{\text{out}}) \log_2(\overline{P}(\phi_{\text{out}})), \tag{2.27}$$

where $\overline{P}(\phi_{\text{out}})$ is the probability of firing at phase ϕ_{out}, averaged over ϕ_{in}, $\overline{P}(\phi_{\text{out}}) = \overline{\lambda}_{\text{out}}/(2\pi\omega)$.

This calculation in principle could be extended to take into account situations in which more than one spike is emitted in a cycle. In order to do this, it is necessary to calculate the conditional probability of multiple spikes, at phases $\phi_{\text{out},1}$, $\phi_{\text{out},2}$, and so on, given ϕ_{in}, which can be done using the above methods. However, in the analysis presented here, we are interested only in the regime with low output spike rates and therefore require only one output spike per cycle.

3 Results

3.1 Interspike Interval Distribution. The interspike interval distribution is given by equation 2.21, and the typical form of the distribution is

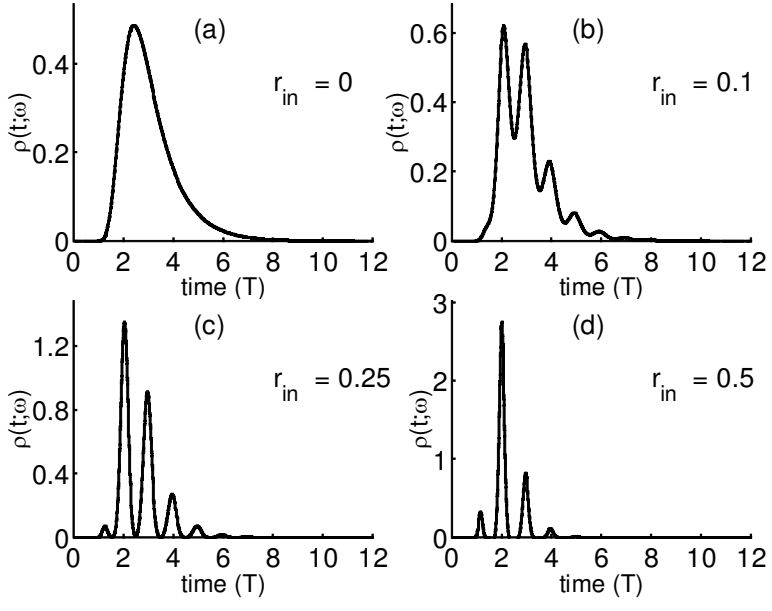

Figure 1: Plots of the interspike interval distribution, $\rho(t;\omega)$, against time (in units of the stimulus period, T) for $N = 64$ inputs, an input frequency of $\omega = 1.0$, average input rate of $\bar{\lambda}_{\text{in}} = 1.0$, and amplitude of the individual EPSPs $a = \theta/64$, where θ is the difference between the threshold and reset values of the potential. Frequency and rate are given as cycles (spikes) per unit of the membrane time constant τ. The four plots are for input synchronizations of (a) $r_{\text{in}} = 0.0$, (b) $r_{\text{in}} = 0.1$, (c) $r_{\text{in}} = 0.25$, and (d) $r_{\text{in}} = 0.5$.

illustrated in Figure 1 for three different values of the input synchronization. All three plots are for $N = 64$ inputs, average rate of input on each input fiber of $\bar{\lambda}_{\text{in}} = 1.0$, and EPSP amplitudes $a = \theta/64$, where θ is the difference between the threshold and reset values of the potential. Frequency, ω, and rate, λ, are measured here in units of the time constant of the membrane, τ, that is, a frequency (rate) of 1.0 corresponds to one cycle (spike) per τ units of time, and the input rate is given by the time-varying function $\lambda(t)$ in equation 2.4. Figure 1a shows the ISI distribution where there is no input synchronization, $r_{\text{in}} = 0$, which is the typical ISI distribution in response to a homogeneous Poisson input (Burkitt & Clark, 2000). Figures 1b, 1c, and 1d show the ISI distributions for inhomogeneous Poisson input with input synchronization $r_{\text{in}} = 0.1, 0.25, 0.5$, respectively. These plots show a multimodal response typical of those recorded, for example, in response to low-frequency acoustical stimulation (less than 1 kHz) in the auditory nerve (Rose et al., 1967). As the input synchronization is increased, the peaks in the

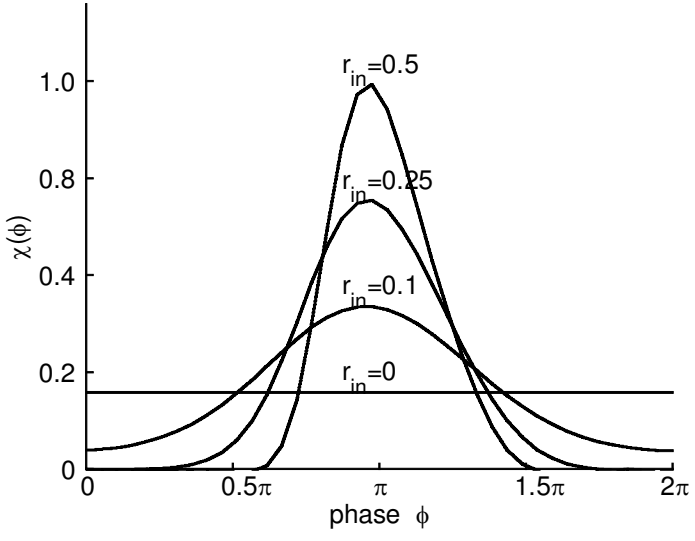

Figure 2: Plots of the period distribution, $\chi^s(\phi)$, (the stationary spike phase density, equation 2.24 for $N = 64$ inputs, an input frequency of $\omega = 1.0$, input rate of $\bar{\lambda}_{\text{in}} = 1.0$, and the amplitudes of the individual EPSPs $a = \theta/64$. The four plots are for input synchronizations of $r_{\text{in}} = 0.0, 0.1, 0.25, 0.5$ as labeled, and have been phase-shifted so that all peaks are at the same phase.

ISI distribution become more pronounced, with each peak corresponding to one cycle of the inputs.

The period distributions of the spike times are plotted in Figure 2 for the four sets of parameters used in Figure 1. The synchronization indices of the output spikes in these four cases are $r_{\text{out}} = 0$ for Figure 1a with $r_{\text{in}} = 0$, $r_{\text{out}} = 0.46$ for Figure 1b with $r_{\text{in}} = 0.1$, $r_{\text{out}} = 0.78$ for Figure 1c with $r_{\text{in}} = 0.25$, and $r_{\text{out}} = 0.90$ for Figure 1d with $r_{\text{in}} = 0.5$. This solution for the stationary spike phase density, equation 2.22, was found by discretizing each period of the inputs into 40 time steps and solving the resulting eigenvalue equation. In Figure 2, the peaks of the distributions have been shifted to a phase of π in order to facilitate their comparison.

For a given set of neural parameters (N, a, θ) and no input synchronization, $r_{\text{in}} = 0$, variations in the average input rate, $\bar{\lambda}_{\text{in}}$, cause the average rate of output spikes, $\bar{\lambda}_{\text{out}}$, to vary in a monotonic fashion. In the limit of a large number of input fibers, $N \to \infty$, there is a critical value of the input rate, $(\bar{\lambda}_{\text{in}})_{\text{crit}}$, below which the average rate of outputs vanishes (Burkitt & Clark, 2000):

$$(\bar{\lambda}_{\text{in}})_{\text{crit}} = \frac{\theta}{Na\tau}. \tag{3.1}$$

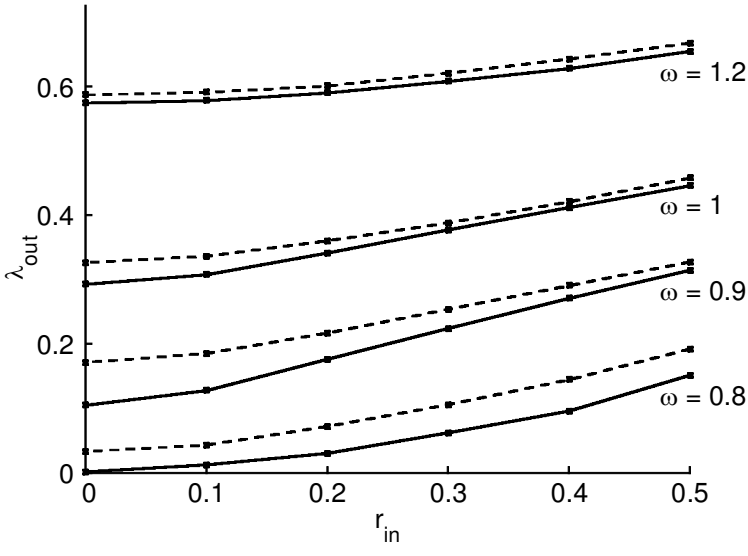

Figure 3: Plot of the average rate of output, $\bar{\lambda}_{out}$, as a function of the synchronization index of the input r_{in} for $N = 64$ (dotted lines) and $N = 128$ (solid lines) inputs, for input frequencies of $\omega = 0.8, 0.9, 1.0, 1.2$ (the average input rate, $\bar{\lambda}_{in}$, is equal to the frequency, ω, namely 1 spike per period of the inputs). The amplitudes of the individual EPSPs are $a = \theta/N$.

For finite values of N, when the synchronization of the inputs increases in this "subcritical" situation (when $\bar{\lambda}_{in} < (\bar{\lambda}_{in})_{crit}$) the coincident arrival of the inputs can result in a nonvanishing rate of outputs (Kempter et al., 1998). This is illustrated in Figure 3, in which the average rate of outputs, $\bar{\lambda}_{out}$, is plotted as a function of the input synchronization, r_{in}, for $N = 64$ (dotted lines) and $N = 128$ (solid lines) and a range of values of the input frequencies (the average input rates here are 1 spike per period in all cases, so that $\bar{\lambda}_{in} = \omega$). The plotted points are the results of the analytical solution, which are connected by the plotted lines for the various values of ω shown on the figure. The results show that an increase in the synchronization of the input, while keeping the average input rate constant, leads to an increase in the average output rate. The effect on the interspike interval distribution is illustrated in Figure 4, in which the neural parameters have the same values as in Figure 1 but the input frequencies (and input rates) take the values of $\omega = 0.9$ (left plot) and 0.8 (right plot), and the resulting output synchronization indices are $r_{out} = 0.91, 0.92$ respectively. Consequently, the effect of a reduction in the frequency and average rate of inputs is both to decrease the average rate of output spikes and increase the number of peaks in the ISI distribution.

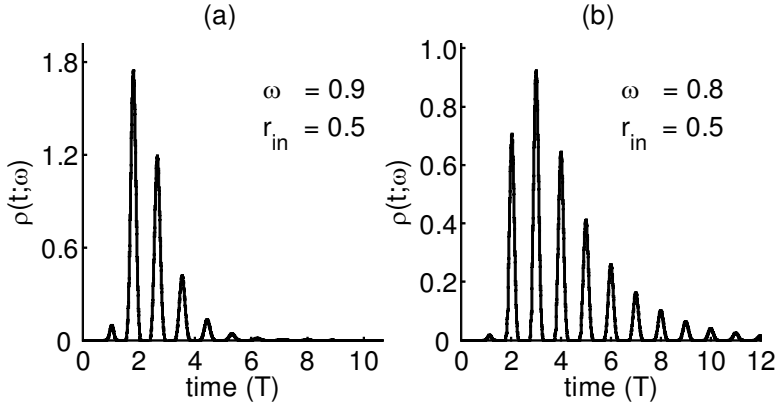

Figure 4: Plots of the interspike interval distribution, $\rho(t;\omega)$, against time (in units of the stimulus period, T) for $N = 64$ inputs. The average input rate is $\bar{\lambda}_{\text{in}} = \omega$, input synchronization is $r_{\text{in}} = 0.5$, and amplitudes of the individual EPSPs are $a = \theta/64$. The input frequencies are (a) $\omega = 0.9$ and (b) 0.8.

3.2 Analysis of Synchronization. The dependence of the synchronization index of the output spikes on the frequency of the time-varying rate of inputs is illustrated in Figure 5, which shows how the synchronization index decreases for increasing frequencies. The average rate of the inputs, $\bar{\lambda}_{\text{in}}$, in this plot is the same as the frequency, that is, there is on average one incoming spike per fiber per cycle of the inputs. For each of the four values of $N = 16, 32, 64, 128$, the amplitude of the individual EPSPs is given by $a = \theta/N$, where θ is the difference between the threshold and reset values of the potential. The synchronization index is large for all cases in this plot and closest to one when the number of inputs is greatest (the case $N = 128$ in Figure 5). The synchronization index of the sinusoidal input rate is $r_{\text{in}} = 0.5$, so that the outputs represent an enhancement of the synchronization relative to the input. The cutoff on the low-frequency side of the plot is determined by the vanishing of the probability of firing (no output spike being produced), and on the high-frequency side, values are plotted up to where the entrainment approaches 100% (output spikes always being generated in the first cycle of the inputs).

The reduction of the output synchronization at higher frequencies observed in Figure 5 is predominantly caused by the resultant high input rate, since the input rate on each fiber was chosen to average one spike per cycle of the input. Figure 6 shows the relationship between the synchronization index of the output spikes with the frequency of the inputs when the average rate of inputs is kept constant, $\bar{\lambda}_{\text{in}} = 1.0$. The decrease in output synchronization with increasing frequency is much more gradual in this case. The nonmonotonic part at lower frequencies is ascribed to resonance effects that

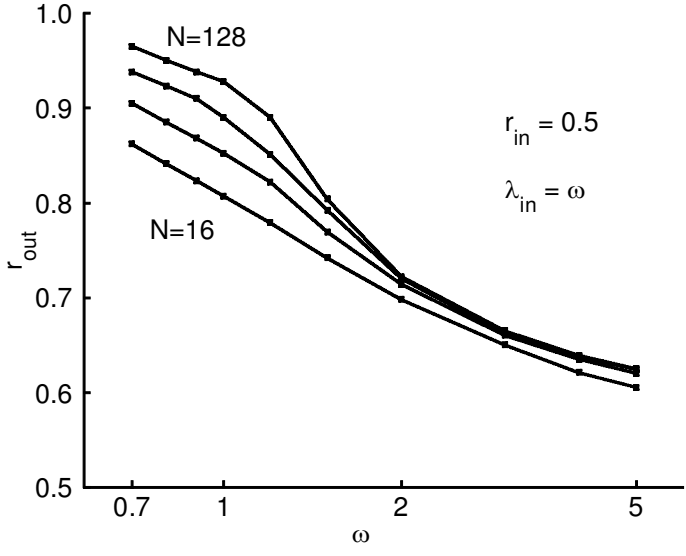

Figure 5: The synchronization index of the output, r_{out}, is plotted against the frequency of the input, ω (measured in units with $\tau = 1$), for a sinusoidally varying rate of inputs with synchronization index $r_{\text{in}} = 0.5$. The amplitude of individual EPSPs is $a = \theta/N$. The average input rate, $\bar{\lambda}_{\text{in}}$, is the same as the frequency in all cases, and the numbers of inputs on the plot are $N = 16$, 32, 64, 128.

occur when the width of the EPSPs is of the same order as the period of the inputs (Kempter et al., 1998).

The dependence of the synchronization index on the synchronization index of the input, r_{in}, is illustrated in Figure 7 for a frequency of $\omega = 1.0$ and an average input rate of $\bar{\lambda}_{\text{in}} = 1.0$ (one spike per input fibre per cycle). The synchronization index of the input, equation 2.4, varies from 0.0 to 0.5, so that all points on the plot show a greater degree of synchronization of the output than is evident in the input. This enhancement of synchronization is more pronounced for large numbers of inputs.

In the subcritical case discussed in section 3.1 where $\bar{\lambda}_{\text{in}} < (\bar{\lambda}_{\text{in}})_{\text{crit}}$, this enhancement of synchronization is more pronounced, as can be seen in Figure 7b. In this plot, the neural parameters have the same values as in Figure 7a, but the input frequency and rate are $\omega = \bar{\lambda}_{\text{in}} = 0.9$, below the critical value of 1.0. This same pattern of enhancement of synchronization for subcritical rates of input is also illustrated in Figure 8, for which $(\bar{\lambda}_{\text{in}})_{\text{crit}} = 0.5$.

The primary factor in the observed enhancement of synchronization is the rate of inputs. This is illustrated in Figure 9, in which the top left plot shows that results for the case where the input frequency and rate are the

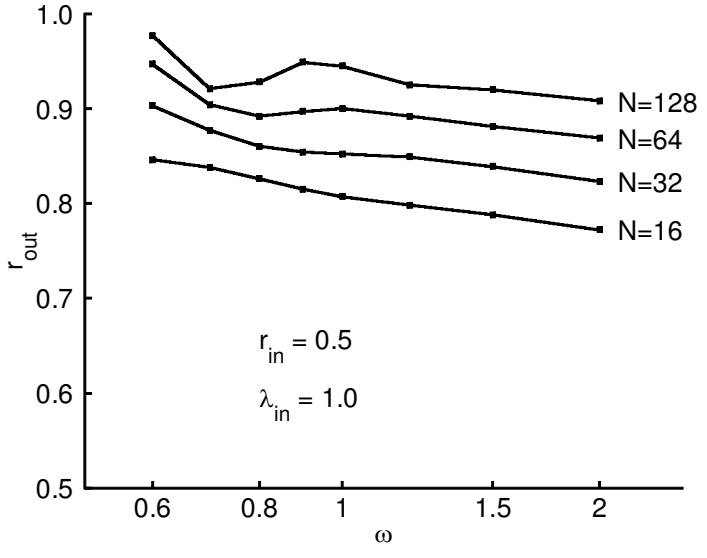

Figure 6: The synchronization index of the output, r_{out}, is plotted against the frequency, ω (measured in units with $\tau = 1$), for a sinusoidally varying rate of inputs with synchronization index $r_{\text{in}} = 0.5$. The amplitude of individual EPSPs is $a = \theta/N$. The average input rate is kept constant, $\bar{\lambda}_{\text{in}} = 1.0$, and the numbers of inputs on the plot are $N = 16, 32, 64, 128$.

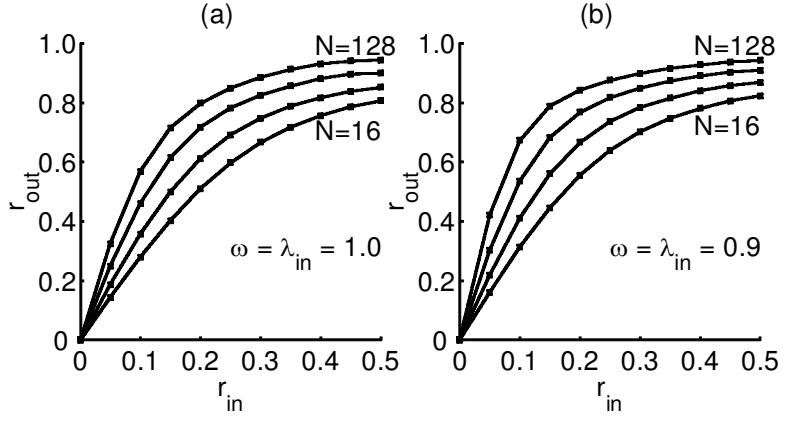

Figure 7: The output synchronization index, r_{out}, is plotted as a function of the input synchronization index, r_{in}, for (a) a frequency of $\omega = 1.0$ and average input rate $\bar{\lambda}_{\text{in}} = 1.0$ (in units with $\tau = 1$) and (b) a frequency of $\omega = 0.9$ and average input rate $\bar{\lambda}_{\text{in}} = 0.9$. The amplitude of individual EPSPs is $a = \theta/N$. The number of inputs on both plots is $N = 16, 32, 64, 128$ (bottom to top plots, respectively).

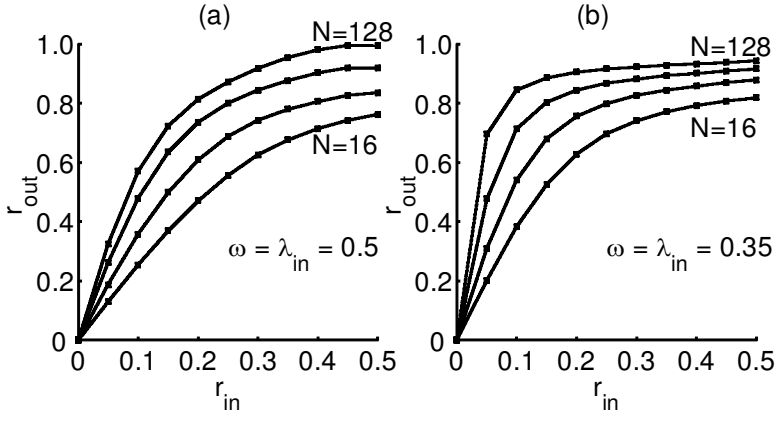

Figure 8: The output synchronization index, r_{out}, is plotted as a function of the input synchronization index, r_{in}, for $N = 16, 32, 64, 128$ (bottom to top plots, respectively). The amplitude of the individual EPSPs is $a = \theta/2N$. The input rate, $\bar{\lambda}_{\text{in}}$, and frequency, ω, are the same in each plot, with (a) $\omega = \bar{\lambda}_{\text{in}} = 0.5$ and (b) $\omega = \bar{\lambda}_{\text{in}} = 0.35$.

same, and the top right plot shows the results when the average input rate is fixed at $\bar{\lambda}_{\text{in}} = 1.0$ for all four frequencies. The plots clearly indicate that it is the reduction in the input rate that leads to the enhancement of synchronization at subcritical input rates.

A comparison of the results obtained using the analysis of section 2 with the results from numerical simulations is presented in Figure 10. The plots show the output synchronization index for a number of inputs ranging from $N = 16$ to 1024 and two values of the input synchronization index, $r_{\text{in}} = 0.1, 0.2$, and with an input rate and frequency both of 1.0. The results of the numerical simulation are connected by the dotted line, and the error bars are the statistical error over simulations with 10,000 output spikes, which decrease as the number of inputs, N, increases. The agreement between the two sets of results increases for larger values of N.

3.3 Analysis of Mutual Information. The above results indicate that a subthreshold mean rate of input, $\bar{\lambda}_{\text{in}} < (\bar{\lambda}_{\text{in}})_{\text{crit}}$, generates an output synchronization, r_{out}, which increases as the number of input fibers, N, is increased. However, in this regime, the average output rate of firing, $\bar{\lambda}_{\text{out}}$, decreases dramatically, as shown in Figure 3. Both quantities, $\bar{\lambda}_{\text{out}}$ and r_{out}, provide some indication of the amount of sensory information that a sensory mechanism can extract from its input. The question then remains, How much information can be gained from subthreshold input on the basis of the output spikes that it generates? We address this question using the mutual

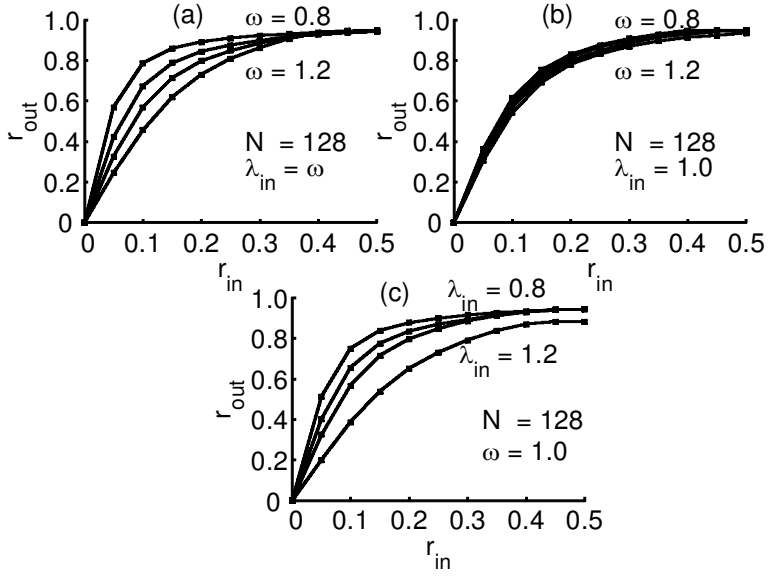

Figure 9: The synchronization index, r_{out}, is plotted as a function of the synchronization index of the input, r_{in}, for $N = 128$ inputs. The amplitude of individual EPSPs is $a = \theta/N$. The average input rate and frequency are (a) equal, $\bar{\lambda}_{in} = \omega$ (average of one input spike per period), (b) constant average input rate at $\bar{\lambda}_{in} = 1.0$ with frequencies $\omega = 0.8$, 0.9, 1.0, and 1.2 (top to bottom plots, respectively, in both *a* and *b*), and (c) constant frequency at $\omega = 1.0$ with average input rates $\bar{\lambda}_{in} = 0.8$, 0.9, 1.0, and 1.2.

information I_M between the input phase of the stimulus and the timing of the output spikes, as described in section 2.6.

For subthreshold input, Figure 11 shows how the mutual information decreases as the input rate decreases and as the number of inputs increases. The range of parameters plotted in this figure is limited to the regime in which the average output spike rate is low, in order that the probability of there being one output spike per cycle is low (and the probability of two output spikes in one cycle is negligible), as required by the approximation of the mutual information (see section 2.6). These results indicate that although the output synchronization increases when there is a small number of output spikes, the amount of information that can be gained about the phase of the input signal decreases. Likewise, although the results illustrated in Figures 6, 7, 8, and 10 indicate that the output synchronization increases with increasing N (and, hence, decreasing postsynaptic amplitude a), the mutual information between the input phase and spike time decreases.

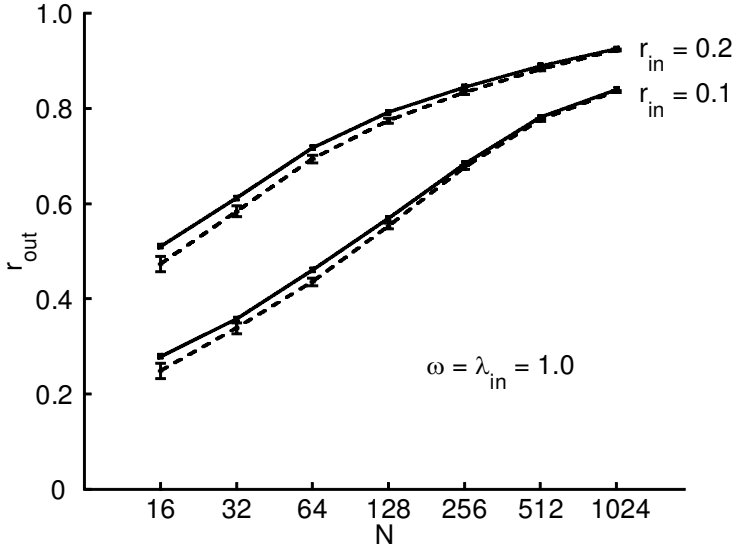

Figure 10: The output synchronization index, r_{out}, is plotted as a function of the number of input fibers, N, for two values of the input synchronization index, $r_{\text{in}} = 0.1, 0.2$. The frequency is $\omega = 1.0$ and average input rate $\bar{\lambda}_{\text{in}} = 1.0$ (in units with $\tau = 1$). The amplitude of individual EPSPs is $a = \theta/N$. The solid line connects the results of the solution using the first passage time density, and the dotted line connects the results of a numerical simulation, with the error bars representing the statistical error for 10,000 output spikes.

4 Discussion

The analysis presented in this study establishes the relationship between both the timing and average rate of spike outputs using the gaussian approximation in an integrate-and-fire neuron with the neural parameters (number of afferent fibers N, PSP amplitudes a, threshold θ, membrane time constant τ) and the input parameters of the periodically modulated spike input (frequency ω and average rate $\bar{\lambda}_{\text{in}}$). For any given set of parameters, the ISI distribution may be evaluated, and representative plots are given in Figures 1 and 4. The period distribution may be evaluated, as illustrated in Figure 2. The relationship between the average rate of the output spikes, $\bar{\lambda}_{\text{out}}$, and the degree of synchronization of the input spikes is illustrated in Figure 3 for a number of frequencies. The frequency dependence of the synchronization of the output spikes is shown in Figures 5 and 6 for the two cases where the input rate is the same as the input frequency (an average of one spike per cycle of the modulated rate) and the input rate is kept fixed as the frequency varies. In each case, the effect of

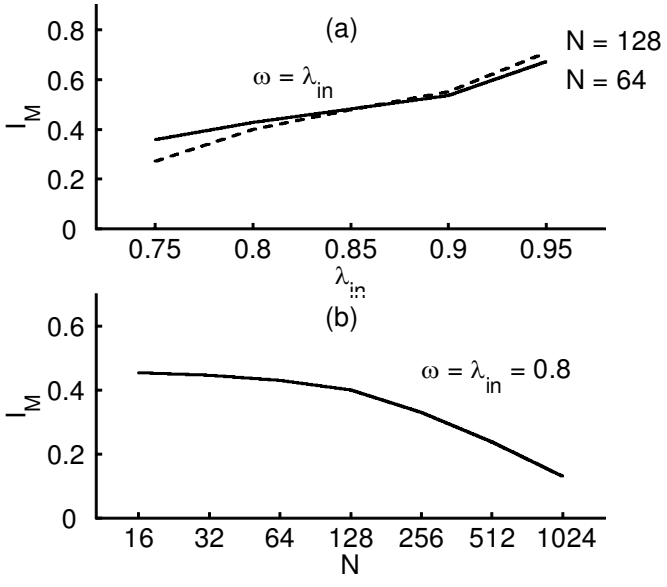

Figure 11: The mutual information, I_M, is plotted as (a) a function of the average input rate, $\bar{\lambda}_{\text{in}}$, for two values of the number of inputs, $N = 64$ (solid line), 128 (dashed line), and (b) a function of the number of inputs with $\bar{\lambda}_{\text{in}} = 0.8$. In both plots, the frequency is $\omega = \bar{\lambda}_{\text{in}}$ (in units with $\tau = 1$), and the input synchronization index is $r_{\text{in}} = 0.5$. The amplitude of individual EPSPs is $a = \theta/N$.

increasing the number of incoming fibers is to increase the synchronization index of the output spikes. The importance of the critical input rate, which may equivalently be formulated as a critical threshold (Kempter et al., 1998) is demonstrated in Figures 7b and 8, which show that the output synchronization is enhanced for subcritical input rates. That this subcritical enhancement is due primarily to the average input rate and not the frequency is illustrated in Figure 9. The results obtained with our method are compared with the results of numerical simulations in Figure 10, which shows that the method becomes more accurate as the number of inputs increases.

However, the higher synchronization of the output spikes observed for smaller input rates $\bar{\lambda}_{\text{in}}$ and larger N (or equivalently, smaller a) *cannot* be interpreted as meaning that the neuron functions optimally in this regime. The calculation of the mutual information between the input phase and output spike times in this regime indicates that the mutual information decreases as the number of inputs increases, as shown in Figure 11. The rapid decrease in the number of output spikes in this regime is responsible for the observed decrease in the amount of mutual information.

This study extends that of earlier studies of coincidence detection and the neural response to noisy periodic synaptic input in a number of important ways. Many of the earlier examinations of the question of coincidence detection were numerical, in which the response to a train of spike inputs was simulated, using either a threshold model with a shot-noise response (Colburn, Han, & Culotta, 1990; Carney, 1992; Joris, Carney, Smith, & Yin, 1994; Diesmann, Gewaltig, & Aertsen, 1999) or a membrane-conductance model (Murthy & Fetz, 1994; Rothman, Young, & Manis, 1993; Rothman & Young, 1996). The results of such simulations are, of course, subject to statistical uncertainties in the accuracy of the results obtained and frequently involve massive computational resources, which limits the parameter space that can be explored. Nevertheless, such studies have been instrumental in establishing many of the central features of the neural response, such as the importance of the convergence of inputs to the postsynaptic neuron and the effect of the coincident arrival of the inputs (Joris et al., 1994). A comprehensive analytical study of the effect of noisy periodic spike input to an integrate-and-fire neuron has been carried out (Kempter et al., 1998), in which the relationship between the input and output rates over the range of input synchronization is analyzed and the conditions under which a neuron can act as a coincidence detector are identified by analyzing the coherence gain and the quality factor for coincidence detection. Their analysis, however, centered on the rate at which output spikes were generated and did not give detailed information on the timing of individual output spikes. The results presented here extend their study by providing an analysis of the timing distribution of output spikes in relation to the phase of the periodic input. Our analysis enables us to find the interspike interval distribution of the output spikes, the synchronization index of the outputs, and the phase distribution of the outputs.

The results presented here illustrate some of the features of stochastic resonance—namely, how the presence of noise can enhance the response of a threshold system to a subthreshold signal. Stochastic resonance, which was originally proposed as an explanation for the ice ages (Benzi, Sutera, & Vulpiani, 1981), has been found to play a role in the sensory pathways of various organisms (Douglas et al., 1993; Braun, Wissing, Schaefer, & Hirsch, 1994). Stochastic resonance has been extensively studied using a two-well potential model in which, in the absence of both noise and external forcing, there are two stable solutions. If the periodic external forcing (signal) is not sufficiently large to overcome the potential barrier, then the system remains in its initial state, while in the presence of noise, the system may jump between the two states at random times. Such transitions are found to be correlated with the (subthreshold) signal and cause a peak in the power spectrum at the frequency of the signal (Benzi et al., 1981). In this way, an increase in the noise can cause an improvement in the output signal-to-noise ratio. The resemblance between interspike interval

histograms and the residence-time distributions of noisy driven bistable systems led to the application of stochastic resonance to neural systems (Bulsara et al., 1991; Longtin, 1993; Chialvo & Apkarian, 1993; Moss, Douglas, Wilkens, Pierson, & Pantozelou, 1993; Bulsara, Elston, Doering, Lowen, & Lindenberg, 1996; Stemmler, 1996; Chialvo et al., 1997, and in particular to the integrate-and-fire neural model (Plesser & Geisel, 1999a, 1999b; Shimokawa et al., 1999). The results presented in Figures 7b and 8b show that the synchronization index of the output spikes for subcritical inputs (see section 3.2) is enhanced relative to that of critical or supracritical inputs, and thus show that stochastic resonance plays a role (Hohn & Burkitt, 2001).

There are a number of approximations in the analysis presented here whose effect requires closer examination. Some of the strengths and shortcomings of the integrate-and-fire model were discussed in section 1, such as the lack of specific currents that underlie spiking and the linear nature of the summation of the postsynaptic responses. The model therefore does not incorporate any of the postulated nonlinear effects in the dendritic tree (Softky, 1994), nor is it capable of modeling the dynamic nature of synapses (Tsodyks & Markram, 1997; Abbott, Varela, Sen, & Nelson, 1997). The gaussian approximation used in this analysis requires that the amplitude of the individual PSPs be small, since the higher-order terms in equations 2.8 and 2.16 are neglected. This is a reasonable approximation in situations where many EPSPs are required to reach threshold, and the comparison with the results obtained by numerical simulation in Figure 10 indicates excellent agreement in the case where there is a large number of small-amplitude inputs. The expression for the conditional first-passage time density, equation 2.12, is exact for situations where the inputs are uncorrelated, but may introduce errors when the presynaptic spikes are not generated by an (inhomogeneous) Poisson process or the synaptic currents have a finite duration (i.e., when more general synaptic response functions are used, such as those that include finite rise times of the postsynaptic response). However, it is straightforward to extend the analysis presented here to other forms of periodically varying input, such as the sum of gaussian distributions (Kempter et al., 1998).

In the analysis presented here, we have ignored the refractory properties of neurons, in which there is a short time immediately following the generation of a spike during which subsequent spikes are suppressed. It is possible to include an absolute refractory period in a straightforward manner by introducing a dead time after a spike is generated, during which incoming postsynaptic potentials have no effect and no further output spike can be generated. We denote this absolute refractory time by τ_{AR}. Its effect is to delay the subsequent summation of the postsynaptic potentials following a spike, and it therefore corresponds to introducing a phase shift of $\phi_{AR} = \omega\tau_{AR}$. The conditional output spike density incorporating this dead time, which we denote by $f_{\theta,AR}(t; \omega, \phi)$, is then simply given by the

phase-shifted original conditional output spike density,

$$f_{\theta,AR}(t;\omega,\phi) = \begin{cases} 0 & \text{for } t < \tau_{AR} \\ f_\theta(t-\tau_{AR};\omega,\phi+\phi_{AR}) & \text{for } t \geq \tau_{AR}, \end{cases} \tag{4.1}$$

such that the summation of the potential starts with a time delay of τ_{AR}, which is also reflected in a shift of the initial phase $\phi \to \phi + \phi_{AR}$.

It is straightforward to extend the analysis presented here to include the effect of a distribution of synaptic strengths and of inhibitory PSPs (Burkitt & Clark, 2000), which is important because of the role that inhibition plays in synchronizing networks of neurons (Nischwitz & Glünder, 1995; Bush & Sejnowski, 1996; White, Chow, Rit, Soto-Treviño, & Kopell, 1998; Neltner, Hansel, Mato, & Meunier, 2000; Tiesinga & José, 2000). It is also possible to include the effect of reversal potentials (Burkitt, 2000, 2001). In order to match the results of the analysis with experimental results of measurements in the auditory pathway, it would also be necessary to consider the distribution of axonal propagation times (i.e., the jitter in the spike travel times along the nerve fibers) that results from differences in axonal lengths, axonal diameters, internodal distances, cell-body area, and cell-body shape (Liberman & Oliver, 1984). This could be done by introducing a timing delay modeled as a gaussian distribution with a width matched to the experimentally observed spread in axonal propagation times, as originally proposed by Anderson (1973) to explain the observed loss of synchronization in auditory nerve spikes with increasing stimulus frequency, that is, the period histogram goes from a pure half-sine-wave distribution at very low frequencies to a completely flat distribution at high frequencies, where all phase information is lost. Even without the inclusion of axonal delays, the results presented here show a fall-off of synchronization with increasing stimulus frequency, although not as rapidly as observed in recordings from the auditory nerve. The results also show the same pattern of increase in synchronization for low output rates that is observed in the auditory nerve (Johnson, 1980), although a more detailed comparison would require the inclusion of the axonal delays.

A model for individual auditory nerve fiber responses enables the modeling of responses of the various cell types in the cochlear nucleus, which is the first stage of processing in the auditory pathway. The enhancement of synchronization observed in the results of this study have also been observed in recordings of the anteroventral cochlear nucleus (AVCN) (Joris et al., 1994). Indeed the low-frequency fibers in the trapezoid body, which is the output tract of the AVCN, show very precise phase locking with synchronization indices that are mostly larger than 0.9 and can approach 0.99 (Joris et al., 1994), which is considerably larger than the synchronization index ever observed in the auditory nerve fibers. The different neural parameters of the various cell types in the cochlear nucleus (and for nuclei in higher stages of the auditory pathway) provide them with different spatiotemporal

summation properties that will be reflected in the temporal characteristics of their spike outputs and the resulting coding of various perceptual features of the acoustic signal (Bruce, Irlicht, & Clark, 1998). For example, it is possible to incorporate systematic differences between the phases of the inputs, such as for modeling inputs from the auditory nerve to neurons in the cochlear nucleus which originate at points distributed along a section of the basilar membrane and therefore have relative phase differences due to the traveling wave of the basilar membrane (Bruce et al., 1998; Kuhlmann, Burkitt, Paolini, & Clark, 2001).

In conclusion, this study quantifies the degree to which the output spikes remain phase-locked to the periodic input, and thus are able to retain and even enhance the temporal information contained in the inputs. The existence of both rate and temporal information in neural transmission and processing plays an important role in the auditory system and possibly in the higher centers of the brain.

Appendix A: Analysis of the Perfect Integrator Neural Model

One of the simplest neural models is the perfect integrator (or leakless integrate-and-fire) model, in which there is no decay of the potential with time. Although neglecting the membrane decay constant is clearly unrealistic, the model nevertheless provides a reasonable approximation when the synaptic inputs summate to threshold over a much shorter timescale than the decay constant.

The solution for the case in which there is a homogeneous Poisson process of rate λ with only excitatory synaptic input follows straightforwardly from the Poisson statistics. If the threshold is reached with m_θ synaptic inputs, where the individual postsynaptic inputs are assumed to have uniform amplitude, then the output spike distribution is exactly the distribution of the m_θ^{th} input,

$$f_{m_\theta}(t) = \frac{\lambda^{m_\theta} t^{m_\theta - 1} e^{-\lambda t}}{(m_\theta - 1)!}. \tag{A.1}$$

The solution of the spike output density for the homogeneous Poisson process with both excitatory and inhibitory inputs may be obtained by using the renewal equation for the first passage time density, obtained using Laplace transforms (Tuckwell, 1988b),

$$f_{m_\theta}(t) = m_\theta \left(\frac{\lambda_E}{\lambda_I}\right) \frac{\exp\{-(\lambda_E + \lambda_I)t\}}{t} I_{m_\theta}(2t\sqrt{\lambda_E \lambda_I}), \tag{A.2}$$

where λ_E, λ_I are the Poisson rates of excitatory and inhibitory inputs, respectively, m_θ is the value of the threshold above the resting potential (in units of the amplitude of the identical individual postsynaptic inputs), and I_m is the modified Bessel function.

A solution may also be obtained by approximating the random arrival times using a Wiener process (Gerstein & Mandelbrot, 1964). The solution for the spike output distribution, again identical to the density of the first passage time to threshold and obtained using the renewal equation and Laplace transforms, is (Gerstein & Mandelbrot, 1964; Tuckwell, 1988b)

$$f_\theta(t) = \frac{\theta}{\sqrt{2\pi\sigma^2 t^3}} \exp\left\{-\frac{(\theta - \mu t)^2}{2\sigma^2 t}\right\}, \tag{A.3}$$

where the threshold is given by $V_{\text{th}} = v_0 + \theta$. The mean and variance are given by

$$\mu = Na\lambda, \qquad \sigma^2 = Na^2\lambda, \tag{A.4}$$

where N is the number of incoming fibers, each with a Poisson rate λ of inputs that have an amplitude a.

The solution for the inhomogeneous Poisson process is derived from the above solution for the homogeneous case by noting that an inhomogeneous Poisson process with a time-dependent rate $\lambda(t)$ can be converted to a standard temporally homogeneous Poisson process by the change in timescale (Tuckwell, 1989),

$$\tau = \int_0^t \lambda(s)\, ds \equiv \Lambda(t). \tag{A.5}$$

This transformation explicitly gives the conditional output spike density at time t:

$$\begin{aligned} f_\theta(t;\, \omega,\, \phi_0) &= \lambda(t) \hat{f}_\theta(\Lambda(t)) \\ &= \frac{\theta\lambda(t)}{\sqrt{2\pi N a^2 \Lambda^3(t)}} \exp\left\{-\frac{(\theta - Na\Lambda(t))^2}{2Na^2\Lambda(t)}\right\}. \end{aligned} \tag{A.6}$$

This expression is valid for any inhomogeneous Poisson process with rate $\lambda(t)$, which is periodic with frequency ω and initial phase ϕ_0.

Inhibitory as well as excitatory inputs can be incorporated into this expression as long as the inhibition has the same rate function $\lambda(t)$. The expressions for μ and σ in the homogeneous (constant rate) case of equation A.3 become

$$\begin{aligned} \mu &= N_E a_E \lambda_E - N_I a_I \lambda_I \\ \sigma^2 &= N_E a_E^2 \lambda_E + N_I a_I^2 \lambda_I, \end{aligned} \tag{A.7}$$

where N_E (N_I) are the number of excitatory (inhibitory) incoming fibers, each with a Poisson rate of intensity λ_E (λ_I) and amplitude of inputs a_E (a_I).

Consequently when inhibition is included in equation A.6, the expression for Na^2 in both denominators becomes $N_E a_E^2 + N_I a_I^2$ and the term Na in the numerator of the exponential becomes $N_E a_E - N_I a_I$.

The interspike interval distribution is obtained by the appropriate average over the initial phase, as given by equation 2.21, using the stationary spike phase density of the phase transition matrix, as described in section 2.5. For the perfect integrator model, the synchronization index of the output spikes is exactly equal to the synchronization index of the inputs, as is straightforwardly confirmed by numerical simulation.

Appendix B: Numerical Solution of the Volterra Integral Equation

The integral equation that is to be solved numerically is a Volterra equation of the first kind,

$$g(t) = \int_0^t ds K(t,s)\rho(s), \tag{B.1}$$

which we wish to solve for $\rho(t)$. In the situation here, the function $K(t,s)$ has a singularity of $(t-s)^{-1/2}$. In addition, we wish to evaluate $\rho(t)$ at evenly spaced intervals, since this function is required for the stationary spike phase distribution, which is solved numerically as an eigenvalue problem at equally distributed phases (see section 2.5). The singularity is eliminated by transforming the integration variable to $x = \sqrt{t-s}$ (Press et al., 1992). Consequently,

$$g(t) = \int_0^{\sqrt{t}} dx 2x K(t, t-x^2)\rho(t-x^2), \tag{B.2}$$

and the integrand is now completely regular.

In order to discretize the t-domain of the integral into m evenly spaced intervals of size $h = \frac{t}{m}$, it is necessary to carry out a nonlinear discretization $\hat{h}$ in the x-domain (Press et al., 1992):

$$\begin{aligned} t_k &= kh \\ x_k &= \sqrt{t_m - t_{m-k}} = \sqrt{kh}, \qquad k = 1, 2, \ldots, m \\ \hat{h}_k &= x_k - x_{k-1} = \sqrt{h}(\sqrt{k} - \sqrt{k-1}). \end{aligned} \tag{B.3}$$

The algorithm for calculating the first passage time density $\rho(t)$ is then

$$\begin{aligned} \rho_0 &= 0 \\ \rho_m &= \frac{g_m - \sum_{k=1}^{m-1}(\hat{h}_{m-k} + \hat{h}_{m-k+1})\sqrt{t_m - t_k} K_{m,k}\rho_k}{\hat{h}_1 \mathcal{H}}, \\ m &= 1, 2, \ldots, \end{aligned} \tag{B.4}$$

where

$$\begin{aligned} g_m &= p(V_{\text{th}}, mh \mid v_0; \omega, \phi) \\ \rho_m &= f_\theta(mh; \omega, \phi) \\ K_{m,k} &= p(V_{\text{th}}, mh \mid V_{\text{th}}, kh, v_0) \\ \mathcal{H} &= \lim_{s \to t} \sqrt{t-s}\, p(V_{\text{th}}, t \mid V_{\text{th}}, s, v_0). \end{aligned} \tag{B.5}$$

Acknowledgments

We thank an anonymous referee for proposing the calculation given here of the mutual information. This work was funded by the Cooperative Research Centre for Cochlear Implant, Speech and Hearing Research, the Bionic Ear Institute, and the National Health and Medical Research Council (NHMRC, Project Grant 990816) of Australia.

References

Abbott, L. F., Varela, J. A., Sen, K., & Nelson, S. B. (1997). Synaptic depression and cortical gain control. *Science, 275*, 220–224.

Abeles, M. (1991). *Corticonics: Neural circuits of the cerebral cortex*. New York: Cambridge University Press.

Anderson, D. J. (1973). Quantitative model for the effects of stimulus frequency upon synchronization of auditory nerve discharges. *J. Acoust. Soc. Am., 54*, 361–364.

Benzi, R., Sutera, A., & Vulpiani, A. (1981). The mechanism of stochastic resonance. *J. Phys. A, 14*, L453–L457.

Braun, H. A., Wissing, H., Schaefer, K., & Hirsch, M. C. (1994). Oscillation and noise determine signal transduction in shark multimodal sensory cells. *Nature, 367*, 270–273.

Bruce, I. C., Irlicht, L. S., & Clark, G. M. (1998). A mathematical analysis of spatiotemporal summation of auditory nerve firings. *Information Sciences, 111*, 303–334.

Bulsara, A. R., Elston, T. C., Doering, C. R., Lowen, S. B., & Lindenberg, K. (1996). Cooperative behavior in periodically driven noisy integrate-fire models of neuronal dynamics. *Phys. Rev. E, 53*, 3958–3969.

Bulsara, A., Jacobs, E. W., Zhou, T., Moss, F., & Kiss, L. (1991). Stochastic resonance in a single neuron model: Theory and analog simulation. *J. Theor. Biol., 152*, 531–555.

Burkitt, A. N. (2000). Interspike interval variability for balanced networks with reversal potentials for large numbers of inputs. *Neurocomput., 32–33*, 313–321.

Burkitt, A. N. (2001). *Balanced neurons: Analysis of leaky integrate-and-fire neurons with reversal potentials*. Manuscript submitted for publication.

Burkitt, A. N., & Clark, G. M. (1999). Analysis of integrate-and-fire neurons: Synchronization of synaptic input and spike output in neural systems. *Neural Comput., 11*, 871–901.

Burkitt, A. N., & Clark, G. M. (2000). Calculation of interspike intervals for integrate and fire neurons with Poisson distribution of synaptic inputs. *Neural Comput., 12*, 1789–1820.

Bush, P., & Sejnowski, T. (1996). Inhibition synchronizes sparsely connected cortical neurons within and between columns in realistic network models. *J. Comput. Neurosci., 3*, 91–110.

Carney, L. H. (1992). Modelling the sensitivity of cells in the anteroventral cochlear nucleus to spatiotemporal discharge patterns. *Phil. Trans. R. Soc. Lond., B336*, 403–406.

Chialvo, D. R., & Apkarian, A. V. (1993). Modulated noisy biological dynamics: Three examples. *J. Stat. Phys., 70*, 375–391.

Chialvo, D. R., Longtin, A., & Müller-Gerking, J. (1997). Stochastic resonance in models of neuronal ensembles. *Phys. Rev. E, 55*, 1798–1808.

Colburn, H. S., Han, Y., & Culotta, C. P. (1990). Coincidence model of MSO responses. *Hear. Res., 49*, 335–346.

Cover, T. M., & Thomas, J. A. (1991). *Elements of information theory*. New York: Wiley.

Destexhe, A. (1997). Conductance-based integrate-and-fire models. *Neural Comput., 9*, 503–514.

Diesmann, M., Gewaltig, M. O., & Aertsen, A. (1999). Stable propagation of synchronous spiking in cortical neural networks. *Nature, 402*, 529–533.

Douglas, J. K., Wilkens, L., Pantozelou, E., & Moss, F. (1993). Noise enhancement of information transfer in crayfish mechanoreceptors by stochastic resonance. *Nature, 365*, 337–340.

Douglas, R., & Martin, K. (1991). Opening the grey box. *Trends Neurosci., 14*, 286–293.

Eckhorn, R., Bauer, R., Jordan, W., Brosch, M., Kruse, W., Munk, M., & Reitboeck, H. J. (1988). Coherent oscillations: A mechanism of feature linking in the visual cortex? *Biol. Cybern., 60*, 121–130.

Fauve, S., & Heslot, F. (1983). Stochastic resonance in a bistable system. *Phys. Lett., 97A*, 5–7.

Gammaitoni, L., Hänggi, P., Jung, P., & Marchesoni, F. (1998). Stochastic resonance. *Rev. Mod. Phys., 70*, 223–287.

Gerstner, W., Kempter, R., van Hemmen, J. L., & Wagner, H. (1996). A neuronal learning rule for sub-millisecond temporal coding. *Nature, 383*, 76–78.

Gerstein, G. L., & Kiang, N. Y.-S. (1960). An approach to the quantitative analysis of electrophysiological data from single neurons. *Biophys. J., 1*, 15–28.

Gerstein, G. L., & Mandelbrot, B. (1964). Random walk models for the spike activity of a single neuron. *Biophys. J., 4*, 41–68.

Glass, L., & Mackey, M. C. (1979). A simple model for phase locking of biological oscillators. *J. Math. Biol., 7*, 339–352.

Goldberg, J. M., & Brown, P. B. (1969). Response of binaural neurons of dog superior olivary complex to dichotic tonal stimuli: Some physiological mechanisms of sound localization. *J. Neurophysiol., 32*, 613–636.

Gray, C. M., König, P., Engel, A. K., & Singer, W. (1989). Oscillatory responses in cat visual cortex exhibit inter-columnar synchronization which reflects global stimulus properties. *Nature, 338*, 334–337.

Gray, C. M., & Singer, W. (1989). Stimulus-specific neuronal oscillations in orientation columns of cat visual cortex. *Proc. Natl. Acad. Sci. USA, 86*, 1698–1702.

Hohn, N., & Burkitt, A. N. (2001). Shot noise in the leaky integrate-and-fire neuron. *Phys. Rev. E, 63*, 031902.

Hopfield, J. J. (1995). Pattern recognition computation using action potential timing for stimulus representation. *Nature, 376*, 33–36.

Iyengar, S., & Liao, Q. (1997). Modeling neural activity using the generalized inverse gaussian distribution. *Biol. Cybern., 77*, 289–295.

Jensen, O., & Lisman, J. E. (1996). Hippocampal CA3 region predicts memory sequences: Accounting for the phase precession of place cells. *Learning and Memory, 3*, 279–287.

Johnson, D. H. (1980). The relationship between spike rate and synchrony in responses of auditory-nerve fibers to single tones. *J. Acoust. Soc. Am., 68*, 1115–1122.

Joris, P. X., Carney, L. H., Smith, P. H., & Yin, T. C. T. (1994). Enhancement of neural synchronization in the anteroventral cochlear nucleus. I. Responses to tones at the characteristic frequency. *J. Neurophysiol., 71*, 1022–1036.

Keener, J. P., Hoppensteadt, F. C., & Rinzel, J. (1981). Integrate-and-fire models of nerve membrane response to oscillatory input. *SIAM J. Appl. Math., 41*, 503–517.

Kempter, R., Gerstner, W., van Hemmen, J. L., & Wagner, H. (1998). Extracting oscillations: Neuronal coincidence detection with noisy periodic spike input. *Neural Comput., 10*, 1987–2017.

Kistler, W. M., Gerstner, W., & van Hemmen, J. L. (1997). Reduction of the Hodgkin-Huxley equations to a single-variable threshold model. *Neural Comput., 9*, 1015–1045.

Koch, C. (1999). *Biophysics of computation: Information processing in single neurons*. Oxford: Oxford University Press.

Köppl, C. (1997). Phase locking to high frequencies in the auditory nerve and cochlear nucleus magnocellularis of the barn owl. *J. Neurosci., 17*, 3312–3321.

Kuhlmann, L., Burkitt, A. N., Paolini, A., & Clark, G. M. (2001). *Analysis of spatiotemporal summation in leaky integrate-and-fire neurons: Application to bushy cells in the cochlear nucleus receiving converging auditory nerve fiber input*. Unpublished manuscript. East Melbourne, Victoria: Bionic Ear Institute.

Lánský, P. (1997). Sources of periodical force in noisy integrate-and-fire models of neuronal dynamics. *Phys. Rev. E, 55*, 2040–2043.

Lapicque, L. (1907). Recherches quantitatives sur l'excitation éléctrique des nerfs traitée comme une polarization. *J. Physiol. (Paris), 9*, 620–635.

Liberman, M. C., & Oliver, M. E. (1984). Morphometry of intracellularly labeled neurons of the auditory nerve: Correlations with functional properties. *J. Comp. Neurol., 223*, 164–176.

Longtin, A. (1993). Stochastic resonance in neuron models. *J. Stat. Phys., 70*, 309–327.

Moss, F., Douglas, J. K., Wilkens, L., Pierson, D., & Pantozelou, E. (1993). Stochastic resonance in an electronic Fitzhugh–Nagumo model. *Ann. N.Y. Acad. Sci., 706*, 26–41.

Murthy, V. N., & Fetz, E. E. (1994). Effects of input synchrony on the firing rate of a three-conductance cortical neuron model. *Neural Comput., 6*, 1111–1126.

Neltner, L., Hansel, D., Mato, G., & Meunier, C. (2000). Synchrony in heterogeneous networks of spiking neurons. *Neural Comput., 12*, 1607–1641.

Nischwitz, A., & Glünder, H. (1995). Local lateral inhibition: A key to spike synchronization? *Biol. Cybern., 73*, 389–400.

Papoulis, A. (1991). *Probability, random variables, and stochastic processes* (3rd ed.). New York: McGraw-Hill.

Plesser, H. E., & Geisel, T. (1999a). Bandpass properties of integrate-fire neurons. *Neurocomput., 26–27*, 229–235.

Plesser, H. E., & Geisel, T. (1999b). Markov analysis of stochastic resonance in a periodically driven integrate-fire neuron. *Phys. Rev. E, 59*, 7008–7017.

Plesser, H. E., & Tanaka, S. (1997). Stochastic resonance in a model neuron with reset. *Phys. Lett. A, 225*, 228–234.

Press, W. H., Flannery, B. P., Teukolsky, S. A., & Vetterling, W. T. (1992). *Numerical recipes in Fortran: The art of scientific computing*. Cambridge: Cambridge University Press.

Rescigno, A., Stein, R. B., Purple, R. L., & Poppele, R. E. (1970). A neuronal model for the discharge patterns produced by cyclic inputs. *Bull. Math. Biophys., 32*, 337–353.

Rose, J. E., Brugge, J. F., Anderson, D. J., & Hind, J. E. (1967). Phase-locked response to low-frequency tones in single auditory nerve fibers of the squirrel monkey. *J. Neurophysiol., 30*, 769–793.

Rothman, J. S., & Young, E. D. (1996). Enhancement of neural synchronization in computational models of ventral cochlear nucleus bushy cells. *Aud. Neurosci., 2*, 47–62.

Rothman, J. S., Young, E. D., & Manis, P. B. (1993). Convergence of auditory nerve fibers onto bushy cells in the ventral cochlear nucleus: Implications of a computational model. *J. Neurophysiol., 70*, 2562–2583.

Shimokawa, T., Pakdaman, K., & Sato, S. (1999). Time-scale matching in the response of a leaky integrate-and-fire neuron model to periodic stimulus with additive noise. *Phys. Rev. E, 59*, 3427–3443.

Singer, W. (1993). Synchronization of cortical activity and its putative role in information processing and learning. *Annu. Rev. Physiol., 55*, 349–374.

Softky, W. R. (1994). Sub-millisecond coincidence detection in active dendritic trees. *Neurosci., 58*, 13–41.

Stein, R. B., French, A. S., & Holden, A. V. (1972). The frequency response, coherence, and information capacity of two neuronal models. *Biophys. J., 12*, 295–322.

Stemmler, M. (1996). A single spike suffices: The simplest form of stochastic resonance in model neurons. *Network: Comput. Neural Syst., 7*, 687–716.

Tiesinga, P. H. E., & José, J. V. (2000). Robust gamma oscillations in networks of inhibitory hippocampal interneurons. *Network: Comput. Neural Syst., 11*, 1–23.

Tsodyks, M. V., & Markram, H. (1997). The neural code between neocortical pyramidal neurons depends on neurotransmitter release probability. *Proc. Natl. Acad. Sci. USA, 94*, 719–723.

Tsodyks, M. V., Skaggs, W. E., Sejnowski, T. J., & McNaughton, B. L. (1996). Population dynamics and theta rhythm phase precession of hippocampal place cell firing: A spiking neuron model. *Hippocampus, 6*, 271–280.

Tuckwell, H. C. (1988a). *Introduction to theoretical neurobiology: Vol. 1, Linear cable theory and dendritic structure*. Cambridge: Cambridge University Press.

Tuckwell, H. C. (1988b). *Introduction to theoretical neurobiology: Vol. 2, Nonlinear and stochastic theories*. Cambridge: Cambridge University Press.

Tuckwell, H. C. (1989). *Stochastic processes in the neurosciences*. Philadelphia: Society for Industrial and Applied Mathematics.

Usher, M., Schuster, H. G., & Niebur, E. (1993). Dynamics of populations of integrate-and-fire neurons, partial synchronizaton and memory. *Neural Comput., 5*, 570–586.

von der Malsburg, C., & Schneider, W. (1986). A neural cocktail-party processor. *Biol. Cybern., 54*, 29–40.

White, J. A., Chow, C. C., Rit, J., Soto-Treviño, C., & Kopell, N. (1998). Synchronization and oscillatory dynamics in heterogeneous, mutually inhibited neurons. *J. Comput. Neurosci., 5*, 5–16.

Received May 16, 2000; accepted February 13, 2001.